Improving thermal stability of novel single-component white-light emitting phosphor $Ca_8MgLu(PO_4)_7$:Tm^{3+}, Dy^{3+} by back-energy-transfer

Feiyan Xie [a,b,1], Dekang Xu [a,1], Zhanchao Wu [c], Maxim S. Molokeev [d,e], Bojana Milićević [b], Hao Li [a], Jianxin Shi [b,*]

[a] *School of Chemistry and Materials Engineering, Huizhou University, Huizhou, 516007, PR China*
[b] *Key Laboratory of Bioinorganic and Synthetic Chemistry of Ministry of Education, School of Chemistry, Sun Yat-Sen University, Guangzhou, 510275, PR China*
[c] *College of Chemistry and Molecular Engineering, Qingdao University of Science &Technology, Qingdao, 266042, PR China*
[d] *Kirensky Institute of Physics, SB RAS, Krasnoyarsk, RU 660036, Russia*
[e] *Siberian Federal University, Krasnoyarsk, 660041, Russia*

ARTICLE INFO

ABSTRACT

The light degradation of WLED devices after long-time use has been proved to be mainly caused by thermal quenching of phosphors, therefore, the design of single-component white-light emitting phosphors with high thermal stability remains a huge challenge. A novel single-phase white light-emitting phosphor $Ca_8MgLu(PO_4)_7$: Tm^{3+},Dy^{3+} was designed and prepared in this work. The photoluminescent results show that white light emission from the phosphor can be achieved by controlling the ratio of Tm^{3+} and Dy^{3+} to adjust the relative intensity of the emission at 451 nm of Tm^{3+} and the emissions at 488, 571 and 660 nm of Dy^{3+}. The luminescence decay results reveal that there is energy transfer from Tm^{3+} to Dy^{3+} in $Ca_8MgLu(PO_4)_7$:Tm^{3+},Dy^{3+} and the efficiency of energy transfer between the two dopants reaches as much as 55%. Temperature-dependent luminescent analyses suggest the highly stable emission of $Ca_8MgLu_{0.76}(PO_4)_7$:$0.12Tm^{3+}$,$0.12Dy^{3+}$ as the integrated emission intensity of the phosphor at 475 K reduces only about 13% of that at room temperature, which is due to the back-energy-transfer from highly doped Dy^{3+} to Tm^{3+} that compensates the luminescence energy. This single-phase white-light emitting phosphor exhibits superior color and luminescence stability and thus may find a potential application in WLEDs.

1. Introduction

In the past decades, white light-emitting diodes (WLEDs) have been extensively studied owing to their superior advantages including energy-saving, high electric-to-optical power efficiency, long lifetime and environmental friendliness, which are considered to be the next generation of solid-state lighting technology for replacing the conventional incandescent and fluorescent lamps [1–3]. Nowadays, the commercial WLEDs are usually fabricated through a combination of the yellow-emitting Ce^{3+}-doped YAG phosphors and blue-emitting GaN LED chips [4–7]. However, this combination suffers low color rendering index and high correlated color temperature due to the lack of red-emitting component in the emission spectrum. To overcome such disadvantages, many researchers are now working on the new combination method, which includes the tri-color-based red-green-blue (RGB) or double-dopants-based phosphors under ultraviolet (UV) or near ultraviolet (NUV) excitation [6–11]. The single-component host matrix can serve as host frameworks for the new combination strategy due to their stable color output as well as their improvement for the luminescence reproducibility and efficiency [12–19]. However, the selection of the single-component host matrix can effectively change the energy transfer, crystal field intensity and the valence bond of activator sites and hence influence the luminescent efficiency, color and intensity stability of phosphors. Therefore, it is urgent to seek suitable single-phase white-emitting phosphors that efficiently prevent the reabsorption of blue light by red and green phosphors.

Among many phosphors, the rare earth-doped inorganic luminescent materials have attracted extensive attention due to their various potential applications in lighting, field emission displays, plasma display panels, and X-ray imaging detectors [20–25]. Phosphates are excellent

---
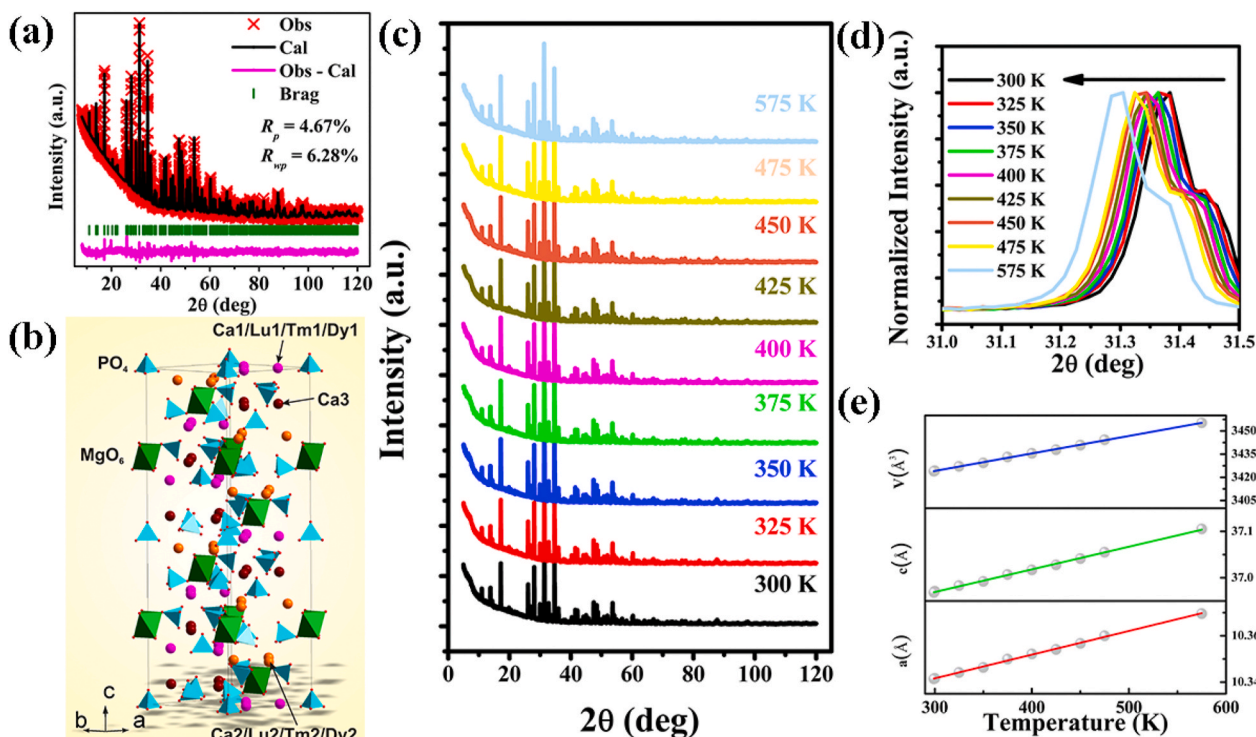
Fig. 1. (a) Structural refinement of CMLP:$0.12Tm^{3+},0.12Dy^{3+}$ at room temperature. (b) Schematic crystal structure of CMLP:$0.12Tm^{3+},0.12Dy^{3+}$ host according to the refinement results. (c) Powder XRD patterns for CMLP:$0.12Tm^{3+}, 0.12Dy^{3+}$ white-light emitting phosphors at different temperatures. (d) The enlarged XRD patterns within the range of 31.0° to 31.5°. (e) Dependence of cell parameters a, c, and V on the increasing temperature.

luminescent hosts for rare-earth dopants due to their stable chemical-physical properties, high thermal stability, low costs and strong absorption in the near ultraviolet region. The whitlockite-type β-$Ca_3(PO_4)_2$ compounds possess six metal ion sites, in which rare earth ions occupy two eight-coordinated sites and a nine-coordinated site, respectively [26,27]. This particular structure can accommodate those ions with similar ionic radii and chemical valence without obviously affecting the structure framework and hence is viewed as excellent host material for single-component white-light-emitting devices. So far, many whitlockite-type compounds, such as rare earth doped $Ca_8MgLa(PO_4)_7$ [28], $Ca_8MgGd(PO_4)_7$ [29], $Ca_8MgY(PO_4)_7$ [30], $Ba_2CaLa(PO_4)_3$ [31] and $Ca_8MgLu(PO_4)_7$ [32] phosphors have been investigated for their synthetic and luminescent properties. We have also prepared Eu^{3+} singly-doped [33] and Tb^{3+}/Eu^{3+} co-doped [34] $Ca_8MgLu(PO_4)_7$ (CMLP) phosphors and studied their pure red and tunable emission properties, respectively. The results show that the CMLP host can accommodate highly doping level of rare earth ions (as much as 100% replacement) and hence exhibits excellent luminescent performance and good thermal stability.

To realize white light for warm WLED devices, the selection of activators is also very important. Dy^{3+} ion is known to be an excellent white light activator due to two dominant emission bands attributed to $^4F_{9/2} \rightarrow {}^6H_{15/2}$ transition (cyan) and $^4F_{9/2} \rightarrow {}^6H_{13/2}$ (yellow). Generally, this ion is able to generate white light in single-phase host. However, since the yellow emission band is sensitive to the host lattice and always becomes dominant in the emission spectrum [35], the compensation of blue emission for Dy^{3+} is essential. Tm^{3+} is one of the blue emitting activators [36] and is found to be an excellent sensitizer for Dy^{3+} ions [37]. The co-doping method has been found in many hosts, such as $NaGd(WO_4)_2$ [38], $K_2Y(WO_4)(PO_4)$ [39], LaF_3 [40], $LiNbO_3$ single crystals [41], $Li_2Gd_4(WO_4)_7$ [42], $NaLaMgWO_6$ [14], and so on. And the above reports present the white light can be generated by adjusting the doping concentrations of Tm^{3+} and Dy^{3+} ions.

As for high-power LEDs, the maintenance of emission intensity at

elevated temperatures is especially required. Generally, one can adopt the doping strategy, such as manipulate the energy transfer paths by altering dopant concentrations [43,44] or modifying the activator sites [45,46], or change the host composition [47–49], in order to reduce thermal quenching. Tm^{3+}/Dy^{3+} co-doping protocol has been reported as mentioned above. However, most of the cases have focused on the low doping level and there is almost no any report on new energy transfer path that efficiently reduces thermal quenching. In the present work, we choose $Ca_8MgLu(PO_4)_7$ as host material for its capacity for doping rare earth ions at a high level and study the condition for white light generation by co-doping Tm^{3+} and Dy^{3+}. The improved thermal stability is found to be mainly attributed to the efficient back-energy-transfer from Dy^{3+} to Tm^{3+}, and the device luminescence properties for WLED of the as-prepared phosphor is preliminarily explored.

2. Experimental

Two series of phosphors with the compositions of $Ca_8MgLu_{1-x}(PO_4)_7$:xTm^{3+} (abbreviated as CMLP:Tm^{3+}) and $Ca_8MgLu_{1-x-y}(PO_4)_7$:xTm^{3+}, yDy^{3+} (abbreviated as CMLP:Tm^{3+},Dy^{3+}) were synthesized by a high temperature solid-state reaction method. The raw materials are $CaCO_3$ (A.R.), $NH_4H_2PO_4$ (A.R.), $(MgCO_3)_4\cdot Mg(OH)_2\cdot5H_2O$ (A. R.), Lu_2O_3 (99.99%), Tm_2O_3 (99.99%) and Dy_2O_3 (99.99%). The raw materials with a stoichiometric ratio were mixed by grinding in an agate mortar. After mixing and grinding, the mixtures were put into crucibles and subsequently heated at 1473 K in a chamber furnace for 3.0 h in air. Finally, the as-synthesized samples were cooled down slowly to room temperature and then ground into powder for measuring.

The structure of the samples was examined on Rigaku D-max 2200 X-ray diffraction (XRD) system with a Cu $K\alpha$ radiation at 30 kV and 30 mA. The photoluminescence (PL), PL excitation spectra and the decay curves at room temperature were measured by FLS 920-Combined Time Resolved and Steady State Fluorescence Spectrometer (Edinburgh Instruments) equipped with a 450 W Xe lamp and a 60 W μF flash lamp,
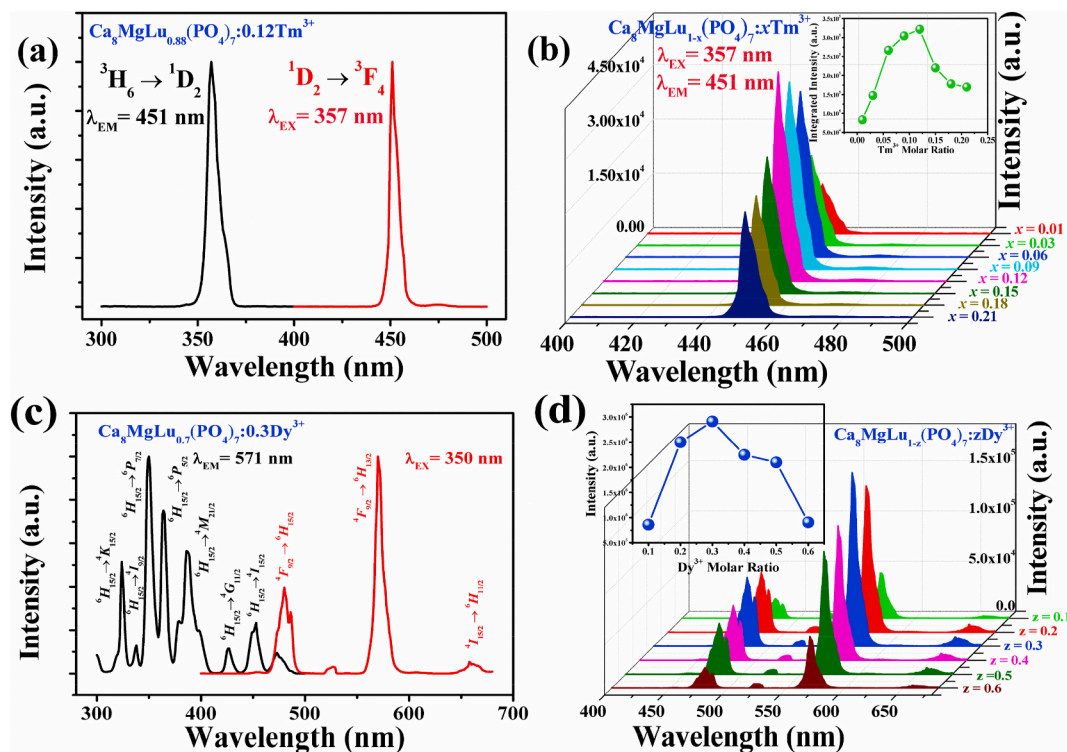
Fig. 2. (a) Normalized excitation and emission spectra of CMLP:0.12Tm^{3+}. (b) Emission spectra of CMLP:xTm^{3+} phosphors (x = 0.01, 0.03, 0.06, 0.09, 0.12, 0.15, 0.18, 0.21) under 357 nm excitation. Inset shows integrated emission intensity of Tm^{3+} as a function of doping concentration. (c) Normalized excitation and emission spectra of CMLP:0.3Dy^{3+}. (d) Emission spectra of CMLP:yDy^{3+} phosphors (y = 0.1, 0.2, 0.3, 0.4, 0.5, 0.6) under 350 nm excitation. Inset shows integrated emission intensity of Dy^{3+} as a function of doping concentration.

respectively. The temperature-dependent PL spectra were performed on the same instrument with a temperature-controller. A UV LED chip with emission peak at 377.7 nm was used to fabricate a WLED device combining the CMLP:0.12Dy^{3+},0.12Tm^{3+} phosphors. CRI measurement and corresponding electroluminescence analysis were conducted on the LED300E programmable test power for LEDs (EVERFINE) with testing current and voltage of 349.8 mA and 3.406 V, respectively.

3. Results and discussion

3.1. XRD analysis

The phase purities of the as-prepared powder samples were examined by XRD. Powder XRD patterns for CMLP, CMLP:0.12Tm^{3+}, CMLP:0.12Dy^{3+}, CMLP:0.12Tm^{3+},0.12Dy^{3+}, and the reference diffraction lines based on the JCPDS card of No. 46–0803 are shown in Fig. S1 (ESI†). The results of XRD analysis confirm that the compounds are of single phase with rhombohedral structure ($R3c$ space group). No extra diffraction peaks related to the starting materials are observed. All the diffraction peaks of the samples can be well indexed to the standard data of CMLP. The XRD results are similar to our previous work [33,34], confirming the successful preparation and good replicability of the adopted high temperature solid state method. From figS1Fig. S1, it is easily found that all the phase structures are similar, but only with peaks shifting to smaller angles, which is caused by the doping lanthanide ions with larger ionic radii. It also confirms the fact that Tm^{3+} and Dy^{3+} ions are successfully doped into the host lattice.

To explore the structure of CMLP, the refinement process at room temperature was performed and is shown in Fig. 1(a). It is found that almost all peaks are well indexed by monoclinic $R3c$ with parameters close to Ca$_9$Eu(PO$_4$)$_7$. Therefore, this structure is taken as starting model for Rietveld refinement. The refined parameters are listed in Tables S1 and S2 (ESI†). The results reveal that three independent Ca sites (Ca1,

Ca2, Ca3) are occupied by Ca^{2+}, Lu^{3+}, Tm^{3+} and Dy^{3+} ions according to suggested chemical formula. Mg^{2+} ion is placed in small octahedral site because it is a preferable site. It is also found that Lu^{3+}/Tm^{3+}/Dy^{3+} ions prefer to occupy only Ca1 and Ca2 sites, and Ca3 site has zero occupancy of Lu^{3+}/Tm^{3+}/Dy^{3+} ions. The crystal structure of CMLP:Tm^{3+},Dy^{3+} is shown in Fig. 1(b) based on the refinement result. It consists of three Ca sites, PO$_4$ tetrahedrons and MgO$_6$ octahedrons. The temperature-dependent XRD patterns (Fig. 1(c)) confirm the fact that the phase structure of the host does not change even in the increasing ambient temperature up to 575 K, only with slight peak shifts towards smaller diffraction angles (Fig. 1(d)). The dependence of cell parameters a, c and V on the increasing temperature in Fig. 1(e) suggests the slight crystal lattice expansion of the host. The above results support the fact that CMLP host is thermally stable structure, which suffers no phase transformation under high ambient temperature.

3.2. Photoluminescence properties of CMLP:Tm^{3+} and CMLP:Dy^{3+}

PL spectra of CMLP:Tm^{3+} phosphors are shown in Fig. 2(a) and (b). The excitation spectra monitored at 451 nm corresponding to $^1D_2 \rightarrow {}^3F_4$ transition of Tm^{3+} are shown in Fig. 2(a). It can only be observed that one excitation band centered at 357 nm in the range of 300–400 nm, which is due to intra-configurational $^3H_6 \rightarrow {}^1D_2$ transition of Tm^{3+}. Under 357 nm excitation, only one emission band attributed to $^1D_2 \rightarrow {}^3F_4$ transition occurs in the blue region. The concentration-dependent luminescent properties of CMLP:Tm^{3+} are also investigated. The corresponding results are shown in Fig. 2(b). All samples display sharp and intense blue emission around 451 nm in the visible light range under UV excitation. The optimal concentration of Tm^{3+} in CMLP phosphor is 12 mol%, demonstrating the relatively large capacity for lanthanide ions doping of CMLP host. The luminescent dynamic analysis is realized by the lifetime measurement (Fig. S2, ESI†). The lifetimes of Tm^{3+} are obtained by fitting the curves with the exponential decay function,
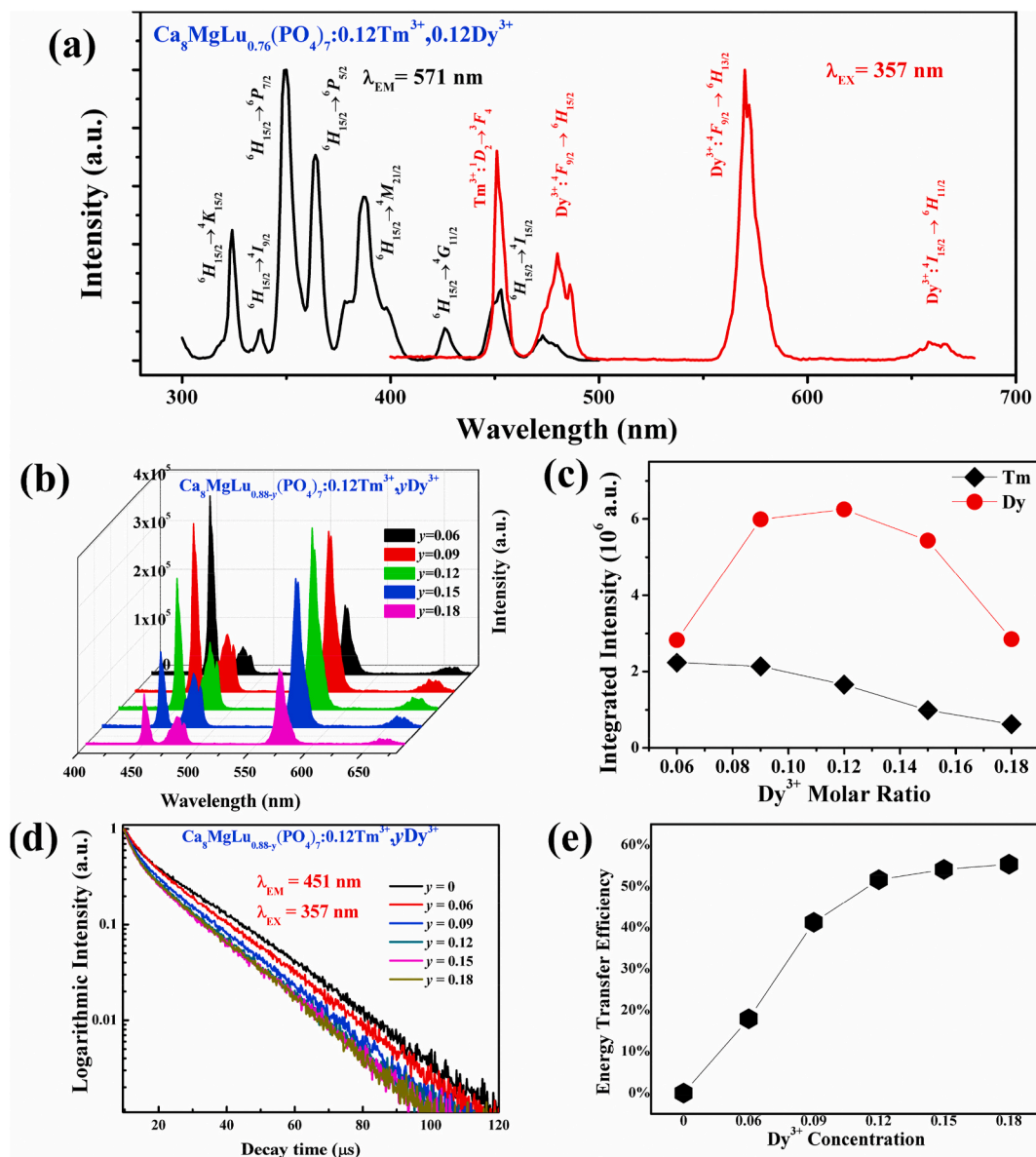
Fig. 3. (a) Normalized excitation and emission spectra of CMLP:$0.12Tm^{3+}$,$0.12Dy^{3+}$. (b) Emission spectra of CMLP:$0.12Tm^{3+}$, yDy^{3+} phosphors (y = 0.1, 0.2, 0.3, 0.4, 0.5, 0.6) under 357 nm excitation. (c) Integrated intensities of Tm^{3+} and Dy^{3+} emission of CMLP phosphors with Dy^{3+} doping concentration. (d) Decay curves $^1D_2 \rightarrow {}^3F_4$ transition of Tm^{3+}. (e) Energy transfer efficiency between Tm^{3+} and Dy^{3+} under 357 nm excitation as a function of y values in CMLP:$0.12Tm^{3+}$, yDy^{3+} (y = 0–0.18).

which is shown as:

$$I = I_0 \exp(-t/\tau) \tag{1}$$

where I and I_0 are the luminescence intensities at time t and 0, respectively, and τ is the luminescence lifetime. We can observe directly a monotonic decrease of Tm^{3+} $^1D_2$ lifetime, indicating the increasing non-radiative rates due to the dominant cross-relaxation process between neighbouring Tm^{3+} ions as Tm^{3+} content is increasing. However, the fact that emission intensity of phosphors increases before Tm^{3+} reaching the optimal concentration suggests that the decreasing theoretical radiative lifetimes can be tailored by increasing Tm^{3+} concentration, which means the radiative rate of Tm^{3+} $^1D_2$ manifold is efficiently enhanced. However, when Tm^{3+} doping concentration keeps increasing, the cross-relaxation process dominates and the non-radiative rates increases remarkably, resulting in the decreasing total lifetime. Moreover, the increasing cross-relaxation process also leads to the reduced emission intensity as shown in Fig. S2 (ESI†). The above results confirm the

optimal Tm^{3+} concentration of 12 mol%, which is used in the following research.

Meanwhile, PL spectra of Dy^{3+} doped CMLP were also measured (see Fig. 2(c) and (d)). It is found that a series of excitation bands attributed to $^6H_{15/2} \rightarrow {}^6P_J$, ^4I_J and ^4G_J transitions of Dy^{3+} occur in CMLP:$0.3Dy^{3+}$. Among all these transitions, $^6H_{15/2} \rightarrow {}^6P_{7/2}$ transition of Dy^{3+} centered at 350 nm is the strongest (Fig. 2(c)). Therefore, we use this wavelength as excitation and obtain the corresponding emission spectra, which consist of three major bands: 488 nm ($^4F_{9/2} \rightarrow {}^6H_{15/2}$, cyan), 571 nm ($^4F_{9/2} \rightarrow {}^6H_{13/2}$, orange) and 660 nm ($^4I_{15/2} \rightarrow {}^6H_{11/2}$, red). Moreover, in Dy^{3+} doped phosphors, site symmetry plays an important role in emission spectra. The ratio between Dy^{3+} cyan and yellow emission intensities reflects the degree of symmetry of Dy^{3+} site in CMLP host matrix. The cyan emission can be realized by the magnetic dipole interaction between Dy^{3+} ions and these transitions are also barely correlated to the chemical environment of the Dy^{3+} ions. The electric dipole transition of Dy^{3+} ions leads to the yellow emission and it can be easily affected by the crystal field around Dy^{3+} ions. If Dy^{3+} ions occupy

the higher symmetry position, the cyan emission intensity will be higher than that of yellow emission. Otherwise, the intensity of cyan emission will be lower [48]. As shown in Fig. 2(d), the yellow emission is higher, which confirms that the Dy^{3+} ions mainly occupy the lower symmetry sites of CMLP host matrix. The spectral analysis of Dy^{3+} emission agrees well with the XRD structural refinement, which exhibits that doped Dy^{3+}/Tm^{3+} ions occupy the lower symmetry sites (Ca1 and Ca2) with eight-coordination, while the nine-coordination site (Ca3) has zero occupancy of Dy^{3+}/Tm^{3+}. Generally, these three bands can generate white light if their proportion is adjusted properly. Therefore, we attempt to investigate the concentration-dependent luminescence, as reflected in Fig. 2(d). It is expected that three major emission bands occur in all samples, with strongest emission intensity at 30% Dy^{3+} molar ratio. We also observe the monotonic decease of lifetimes along with Dy^{3+} concentration (see Fig. S3, ESI†), indicating the non-radiative transition process becomes the dominant depletion mechanism of emissive manifolds, similar to that of Tm^{3+} doping. However, we cannot observe any white light generation in all Dy^{3+}-doped samples (see Fig. S4 and Table S3, ESI†), which is due to the lack of blue emission component. Therefore, co-doping of Tm^{3+} is expected to compensate the blue region and hence results in the white-light emission.

3.3. Photoluminescence properties of CMLP:Tm^{3+},Dy^{3+}

Based on the above analysis, we investigated the co-doping effect of different Dy^{3+} content in CMLP:0.12Tm^{3+} phosphors. Fig. 3(a–c) shows the luminescence properties of CMLP:Tm^{3+},Dy^{3+} phosphors. The excitation spectrum monitored at $^4F_{9/2} \rightarrow {}^6H_{13/2}$ transition of Dy^{3+} shows the almost identical spectral behavior with that of Dy^{3+} singly-doped samples. The excitation behaviours between $^1D_2 \rightarrow {}^3F_4$ transition of Tm^{3+} and $^4F_{9/2} \rightarrow {}^6H_{13/2}$ transition of Dy^{3+} are also compared (see Fig. S5, ESI†). It is found that excitation bands of Dy^{3+} overlap partly with those of Tm^{3+}, which indicates the possible energy transfer between the two dopants. Hence, $^1D_2 \rightarrow {}^3F_4$ transition (357 nm) of Tm^{3+} is used as excitation source in consideration of two reasons: Firstly, Tm^{3+} is regarded as a sensitizer and the energy transfer from Tm^{3+} to Dy^{3+} is explored. Secondly, 357 nm is viewed as nearer NUV than 350 nm of Dy^{3+}. As a result, the emission spectra consist of four emission bands: 488 nm, 571 nm, 660 nm of Dy^{3+} and 451 nm of Tm^{3+}, which differ from the Dy^{3+} singly-doped case. We can also see the remarkable overlap between the emission of Tm^{3+} and the excitation of Dy^{3+} at around 450 nm, which obviously suggests the efficient energy transfer from Tm^{3+} to Dy^{3+}. The above energy transfer process can also be verified by the fact that $^1D_2$ emission intensity of Tm^{3+} is reduced with increasing the doping concentration of Dy^{3+} (Fig. 3(b) and (c)). The emission intensity of Dy^{3+} ions in CMLP:0.12Tm^{3+}, yDy^{3+} increases with increasing the concentration of Dy^{3+} ions and reaches the maximum at 12 mol%. Afterwards, the emission intensity significantly decreases due to the concentration quenching effect that induces cross-relaxation process between the neighbouring Dy^{3+} ions.

To validate the ET efficiency from Tm^{3+} to Dy^{3+}, the luminescence dynamic behavior of different concentration of Dy^{3+} doped CMLP:0.12Tm^{3+} phosphors is studied as shown in Fig. 3(d). Being similar to Tm^{3+} singly-doped situation, the lifetimes of $^1D_2$ manifold of Tm^{3+} decreases along with increasing Dy^{3+} doping content. The ET efficiency from sensitizer to activator can be expressed as [40]:

$$\eta = 1 - \frac{I_S}{I_{S0}} = 1 - \frac{\tau_S}{\tau_{S0}} \tag{2}$$

where τ_S and τ_{S0} represent luminescence decay lifetime of the sensitizer with and without the activator, respectively. To obtain the efficiency, one must acquire the lifetimes of the sensitizer. The lifetimes of $^1D_2$ manifold of Tm^{3+} can be obtained by fitting the luminescence decay curve with the similar decay expression as discussed above. For CMLP:0.12Tm^{3+},yDy^{3+} (y = 0, 0.06, 0.09, 0.12, 0.15 and 0.18), the
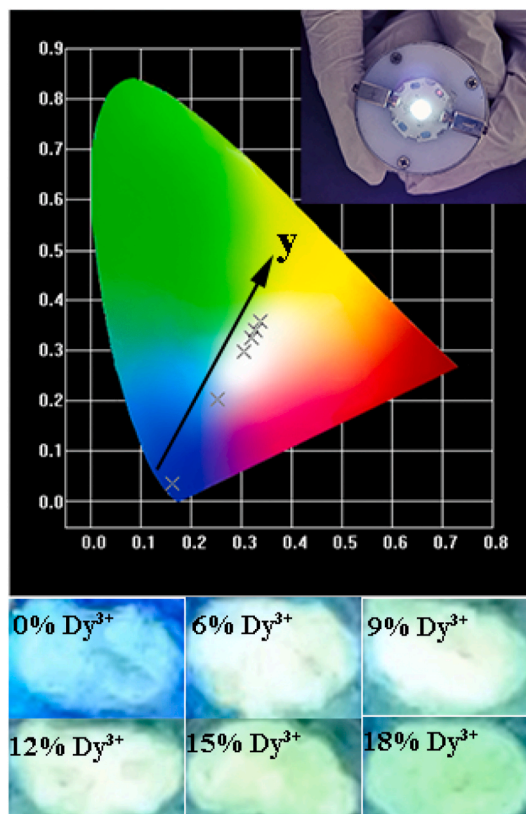

Fig. 4. (Upper panel) CIE chromaticity diagram for CMLP:0.12Tm^{3+},yDy^{3+} (y = 0–0.18) phosphors under 357 nm excitation. (Lower panel) Digital images of corresponding CMLP: 0.12Tm^{3+},yDy^{3+} phosphors. Inset shows the WLED device through the combination of CMLP:0.12Tm^{3+},0.12Dy^{3+} phosphors and a 377.7 nm UV chip.

lifetimes are 12.8, 10.52, 7.53, 6.20, 5.88 and 5.72 μs, respectively. Accordingly, the ET efficiency increases with increasing Dy^{3+} concentration (shown in Fig. 3(e)). The ET efficiency can reach as much as 55%, indicating the highly efficient ET process from Tm^{3+} to Dy^{3+}. Besides, as mentioned above, the overlap excitation range of Tm^{3+} and Dy^{3+} makes it possible for the competition of ET between these two ions [50]. However, it is considered to be the dominant mechanism that the ET occurs from Tm^{3+} to Dy^{3+} (see Fig. S6, ESI†) due to the efficient absorption of Tm^{3+} at around 357 nm compared with Dy^{3+} at around 350 nm (see Fig. S5, ESI†). Quantum yield (QY) was measured through Hamamatsu C9920-03G Quantum Yield System under 360 nm excitation. The QY of CMLP:0.12Tm^{3+},0.12Dy^{3+} is about 29% (see Fig. S7, ESI†), which is quite satisfactory compared to the previous reports on Tm^{3+} and Dy^{3+} co-doped phosphors as shown in Table 2 [14,39,51-53].

3.4. Application of CMLP:0.12Tm^{3+},yDy^{3+} phosphors in WLEDs

Accordingly, the CIE chromaticity coordinates of CMLP:0.12Tm^{3+}, yDy^{3+} phosphors were traced as shown in Fig. 4. It is obviously found that the CIE chromaticity coordinates vary from blue region to white light region. The corresponding CIE chromaticity coordinates are (0.154, 0.021), (0.304, 0.297), (0.311, 0.312), (0.319, 0.325), (0.327, 0.340), and (0.337, 0.357) for samples co-doped with 0, 0.06, 0.09, 0.12, 0.15 and 0.18 Dy^{3+}, respectively. The corresponding correlated color temperature (CCT) is then calculated as shown in Table S4 (ESI†). It is found that the CCT of samples decreases along with increasing Dy^{3+} content, indicating the possible application of the co-doping samples for WLEDs. The digital images (lower panel of Fig. 4) of the corresponding samples also support the results of CIE diagram. A WLED device composed of our products (CMLP:0.12Dy^{3+},0.12Tm^{3+}) and a 377.7 nm
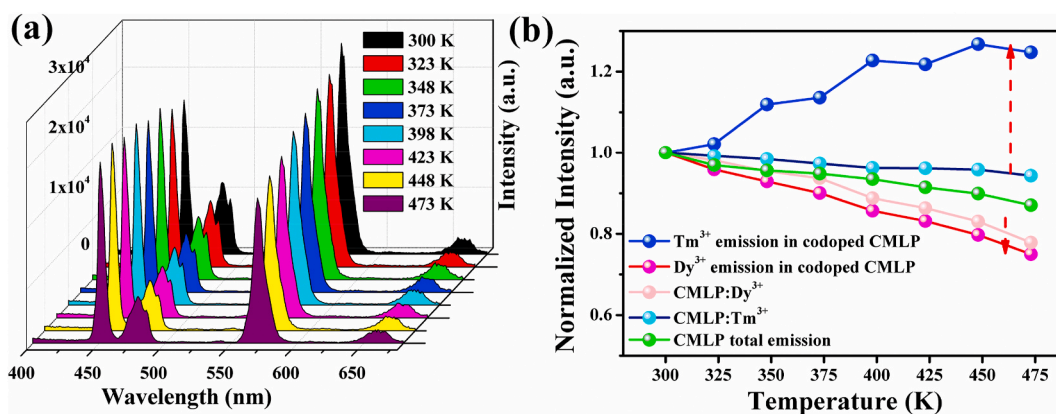
Fig. 5. (a) Temperature-dependent emission spectra of CMLP:0.12Tm^{3+},0.12Dy^{3+} phosphor. (b) The corresponding integrated luminescence of total emission, Tm^{3+} and Dy^{3+} emission of CMLP:Tm^{3+},Dy^{3+}, integrated Dy^{3+} emission of CMLP:Dy^{3+} and integrated Tm^{3+} emission of CMLP:Tm^{3+}, respectively, along with various temperatures compared to 300 K, respectively.
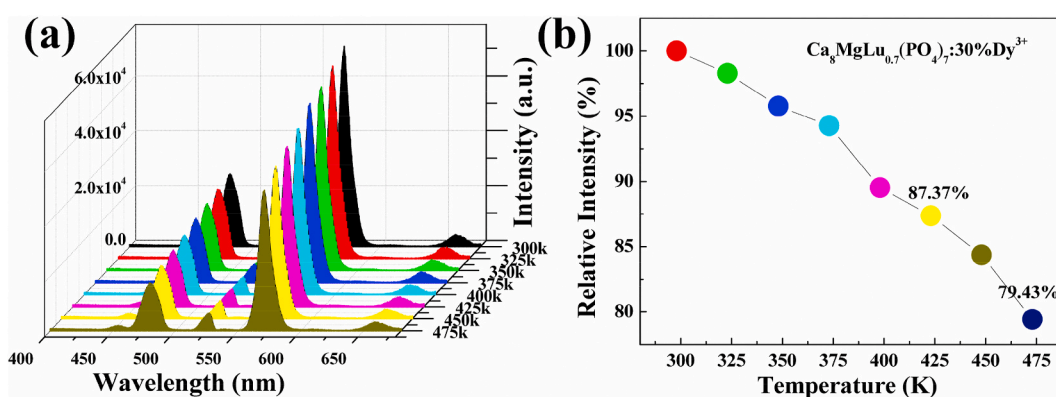

Fig. 6. (a) Emission spectra of CMLP:0.3Dy^{3+} under various temperatures. (b) Dependence of relative intensity of CMLP:0.3Dy^{3+} on temperature.

UV chip is also fabricated (see inset of Fig. 4). The device displays relatively pure white-light emission with the color rendering index (CRI) about 80.2, indicating the superior luminescence performance.

3.5. Improving the thermal stability of CMLP:0.12Tm^{3+},0.12Dy^{3+} by back-energy-transfer

The thermal quenching property is one of the important technological parameters for the application of phosphors because it has a considerable influence on the light output and CRI. The temperature dependence of the emission spectra and their corresponding integrated intensity of CMLP:0.12Tm^{3+}, 0.12Dy^{3+} excited with 357 nm are illustrated in Fig. 5 upon heating the phosphor samples in a temperature range from 300 to 475 K. When the temperature is increased up to 450 and 475 K, the integrated emission intensity is found to be 89.89% and 87.01% of that at 300 K (Fig. 5(b)). Compared with Dy^{3+} singly-doped CMLP phosphor (Fig. 6), the co-doping CMLP phosphor exhibits more stable luminescence in the emission intensity. However, the situation will be a bit different by dividing the integrated luminescence intensity of CMLP phosphor into two parts: Tm^{3+} emission and Dy^{3+} emission. As shown in Fig. 5(b), Tm^{3+} emission increases and Dy^{3+} emission decreases along with elevated temperatures. We also compare Tm^{3+} and Dy^{3+} emission in singly-doped CMLP systems and observe an obvious increase of Tm^{3+} emission and reduction of Dy^{3+} emission by co-doping strategy, respectively. Despite the factor of structural variation with increasing temperature has less influence on the thermal stability of luminescence, the major reason that induces more stable luminescence of CMLP:Tm^{3+},Dy^{3+} is the back-energy-transfer (BET) from Dy^{3+} to Tm^{3+} as the increasing temperature promotes more phonons of the
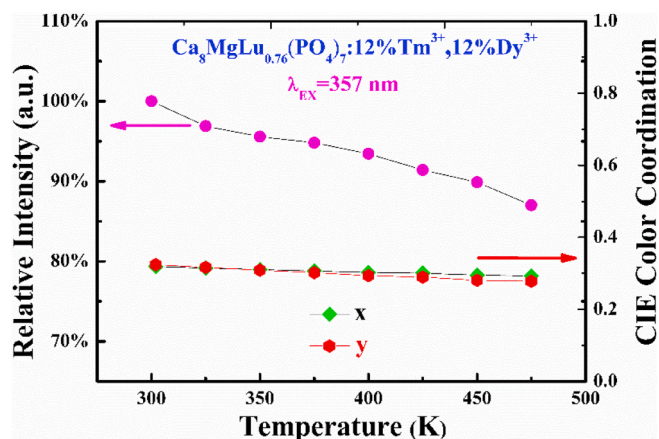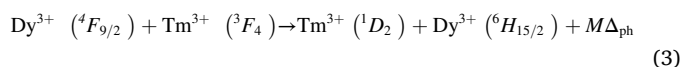

Fig. 7. Integrated luminescence intensity of CMLP:Tm^{3+},Dy^{3+} phosphor and their corresponding chromaticity coordinates along with elevated temperatures.

CMLP host that compensate the BET process [19]. It is proposed that the BET process is considered to be

$$Dy^{3+} \left(^4F_{9/2} \right) + Tm^{3+} \left(^3F_4 \right) \rightarrow Tm^{3+} \left(^1D_2 \right) + Dy^{3+} \left(^6H_{15/2} \right) + M\Delta_{ph}$$

(3)

where Δ_{ph} is the phonon energy; M is the number of involved phonons. Obviously, the rising temperature provides more phonons to promote

Table 1

Calculated chromaticity shift of CMLP:Tm^{3+},Dy^{3+} along with various temperatures.

Temperature (K)	x	y	$\Delta\varepsilon \times 10^{-3}$
300	0.3190	0.3244	0.00
323	0.3149	0.3164	6.95
348	0.3107	0.3088	13.94
373	0.3068	0.3017	20.64
398	0.3023	0.2935	28.59
423	0.3007	0.2899	31.88
448	0.2952	0.2809	41.42
473	0.2933	0.2779	44.72

Table 2

The comparison of quantum yield and thermal quenching effect of our samples and some other single-component white-light emitting phosphors.

Phosphors	Quantum Yield (%)	I_{475K}/I_{300K}	References
$Ca_8MgLu(PO_4)_7$:$0.3Dy^{3+}$	22%	79.43%	This work
$Ca_8MgLu(PO_4)_7$:$0.12Dy^{3+}$,$0.12Tm^{3+}$	29%	87.01%	This work
$Ca_8MgLu(PO_4)_7$:$0.02Ce^{3+}$,$0.64Tb^{3+}$	68%	60%	[32]
$Ca_8MgLu(PO_4)_7$:$0.02Ce^{3+}$,$0.6Mn^{2+}$	20%	60%	[32]
$NaLaMgWO_6$:$0.02Tm^{3+}$,$0.04Dy^{3+}$	–	78%	[14]
$K_2Y(WO_4)(PO_4)$:$0.01Tm^{3+}$,$0.05Dy^{3+}$	16.7%	50%	[39]
$BaY_2Si_3O_{10}$:$0.03Tm^{3+}$,$0.1Dy^{3+}$	40.86%	77.8% for Tm^{3+} and 70.6% for Dy^{3+}	[51]
$K_3Gd(PO_4)_2$:$0.01Tm^{3+}$,$0.08Dy^{3+}$	20.3%	45%	[52]
$LaMgAl_{11}O_{19}$:$0.03Tm^{3+}$,$0.1Dy^{3+}$	–	51%	[53]

the above process and thus enhances the Tm^{3+} emission in the sacrifice of Dy^{3+} emission.

We also checked the stability of the emission color by calculating the CIE coordinates under different temperatures (Fig. 7). It can be found that CIE coordinates decrease slightly along with increased temperatures, confirming the fact that the phosphors possess a good color stability. The color stability can also be quantifiably described by the chromaticity shift ($\Delta\varepsilon$) by using the following equation [54]

$$\Delta\varepsilon = \sqrt{(u_t - u_0)^2 + (v_t - v_0)^2 + (w_t - w_0)^2} \qquad (4)$$

where $u = 4x/(3 - 2x + 12y)$, $v = 9y/(3 - 2x + 12y)$, $w = 1 - u - v$. Subscript t and 0 represent the coordinates at final and initial temperatures. x and y are chromaticity coordinates. The calculated results are shown in Table 1 and Fig. S8 (ESI†). As a result, the chromaticity shift of CMLP:$0.12Tm^{3+}$,$0.12Dy^{3+}$ exhibits a slight increase with elevated temperature and reaches about 44.7×10^{-3} at 473 K. The chromaticity shift of CMLP:$0.12Tm^{3+}$,$0.12Dy^{3+}$ is relatively small that can be considered as stable chromaticity. The above results demonstrate the excellent thermal stability of CMLP:Tm^{3+},Dy^{3+} phosphors. Specifically, the luminescence intensity at 473 K is 87.01% of that at 300 K, which shows better luminescence performance at higher temperature than Dy^{3+} singly-doped CMLP and many other Dy^{3+}-Tm^{3+} co-doped phosphors (see Table 2) [14,39,51-53]. We further explored the temperature-dependent emission to determine the activation energy for thermal quenching (Figs. S9 and S10, ESI†). The experimentally calculated activation energy ΔE is 0.13 eV for CMLP:$0.12Tm^{3+}$,$0.12Dy^{3+}$. The calculated activation energy is smaller than that of CMLP:$0.3Dy^{3+}$, which is probably due to the additional Tm^{3+} that alters the crystal field and hence influences the phonon-assisted energy transfer process. In a word, the above results suggest the excellent thermal stability of CMLP:Tm^{3+},Dy^{3+} phosphors.

4. Conclusions

A series of rhombodedral phosphors $Ca_8MgLu_{1-x-y}(PO_4)_7$:xTm^{3+}, yDy^{3+} have been synthesized by the high temperature solid-state reaction. Upon UV excitation, white-light emission depending on dopant concentrations can be achieved by integrating a blue emission band from Tm^{3+} located at 458 nm and three bands from Dy^{3+} located at 488, 576 and 660 nm. The efficient energy transfer has been proved to occur between Tm^{3+} and Dy^{3+} ions in the phosphors, and the efficiency of the energy transfer between the two dopants is as high as 55%. The quantum yield of the single-host white-light emitting phosphor $Ca_8MgLu_{0.76}(PO_4)_7$:$0.12Tm^{3+}$, $0.12Dy^{3+}$ phosphor is about 29%. Furthermore, benefitting from the back-energy-transfer from highly doped Dy^{3+} to Tm^{3+} that compensates the luminescence energy, the chromaticity shift of the phosphor is only 44.7×10^{-3} at 473 K and the luminescence intensity at 473 K is 87.01% of that at 300 K. The satisfactory quantum yield, the ultra-small chromaticity shift and the superior luminescence stability suggest that the phosphor can be a promising single-component white-light emitting candidate for UV chip pumped WLEDs.

Declaration of competing interest

The authors declare that they have no known competing financial interests or personal relationships that could have appeared to influence the work reported in this paper.

Acknowledgements

Appendix A. Supplementary data

Supplementary data to this article can be found online at https://doi.org/10.1016/j.jlumin.2020.117516.

References

[1] G.B. Nair, H.C. Swart, S.J. Dhoble, Prog. Mater. Sci. 109 (2020), 100622.
[2] Y.-C. Lin, M. Karlsson, M. Bettinelli, Topics Curr. Chem. 374 (2016) 21.
[3] C.C. Lin, R.-S. Liu, J. Phys. Chem. Lett. 2 (2011) 1268–1277.
[4] P. Pust, P.J. Schmidt, W. Schnick, Nat. Mater. 14 (2015) 454–458.
[5] Z.G. Xia, Q.L. Liu, Prog. Mater. Sci. 84 (2016) 59–117.
[6] J.H. Li, J. Yan, D.W. Wen, W.U. Khan, J.X. Shi, M.M. Wu, Q. Su, P.A. Tanner, J. Mater. Chem. C 4 (2016) 8611–8623.
[7] T. Takeda, R.-J. Xie, T. Suehiro, N. Hirosaki, Prog. Solid State Chem. 51 (2018) 41–51.
[8] K. Li, M.M. Shang, H.Z. Lian, J. Lin, J. Mater. Chem. C 4 (2016) 5507–5530.
[9] W.U. Khan, L. Zhou, Q.Y. Liang, X.H. Li, J. Yan, N.U. Rahman, L. Dolgov, S. U. Khan, J.X. Shi, M.M. Wu, J. Mater. Chem. C 6 (2018) 7612–7618.
[10] J.H. Li, Z.H. Zhang, X.H. Li, Y.Q. Xu, Y.Y. Ai, J. Yan, J.X. Shi, M.M. Wu, J. Mater. Chem. C 5 (2017) 6294–6299.
[11] W.U. Khan, S.B. Mane, S.U. Khan, D.D. Zhou, D. Khan, Q.X. Yu, W.J. Zhou, L. Zhou, J.X. Shi, M.M. Wu, RSC Adv. 8 (2018) 40693–40700.
[12] V. Bachmann, T. Justel, A. Meijerink, C. Ronda, P.J. Schmidt, J. Lumin. 121 (2006) 441–449.
[13] M.M. Shang, C.X. Li, J. Lin, Chem. Soc. Rev. 43 (2014) 1372–1386.
[14] Q. Liu, J. Guo, M.H. Fan, Q. Zhang, S. Liu, K.L. Wong, Z.Y. Liu, B. Wei, J. Mater. Chem. C 8 (2020) 2117–2122.
[15] Z.W. Zhang, J.H. Li, N. Yang, Q.Y. Liang, Y.Q. Xu, S.T. Fu, J. Yan, J.B. Zhou, J. X. Shi, M.M. Wu, Chem. Eng. J. 390 (2020), 124601.
[16] N. Liu, L.F. Mei, L.B. Liao, J. Fu, D. Yang, Sci. Rep. 9 (2019) 15509.
[17] R.J. Dong, W. Liu, Y.H. Song, X.T. Zhang, Z.C. An, X.Q. Zhou, K.Y. Zheng, Y. Sheng, Z. Shi, H.F. Zou, J. Lumin. 214 (2019), 116585.
[18] Y.Z. Fang, X.P. Tian, J.H. Liu, Y. Zhang, Y.F. Liu, G.Y. Zhao, J. Zou, N. Vainos, J. S. Hou, J. Lumin. 207 (2019) 34–40.

[19] J.H. Li, Q.Y. Liang, J.-Y. Hong, J. Yan, L. Dolgov, Y.Y. Meng, Y.Q. Xu, J.X. Shi, M. M. Wu, ACS Appl. Mater. Interfaces 10 (2018) 10866–18072.

[20] D.W. Wen, J.J. Feng, J.H. Li, J.X. Shi, M.M. Wu, Q. Su, J. Mater. Chem. C 3 (2015) 2107–2114.

[21] Q.L. Dai, M.E. Foley, C.J. Breshike, A. Lita, G.F. Strouse, J. Am. Chem. Soc. 133 (2011) 15475–15486.

[22] G.M. Cai, N. Yang, H.X. Liu, J.Y. Si, Y.Q. Zhang, J. Lumin. 187 (2017) 211–220.

[23] G.H. Li, N. Yang, J. Zhang, J.Y. Si, Z.L. Wang, G.M. Cai, X.J. Wang, Inorg. Chem. 59 (2020) 3894–3904.

[24] C.M. Liu, Z.M. Qi, C.G. Ma, P. Dorenbos, D.J. Hou, S. Zhang, X.J. Kuang, J. H. Zhang, H.B. Liang, Chem. Mater. 26 (2014) 3709–3715.

[25] X.J. Wang, S. Funahashi, T. Takeda, T. Suehiro, N. Hirosaki, R.J. Xie, J. Mater. Chem. C 4 (2016) 9968–9975.

[26] Y.N. Xue, F. Xiao, Q.Y. Zhang, Spectrochim. Acta Part A 78 (2011) 1445–1448.

[27] A. Bessiere, R.A. Benhamou, G. Wallez, A. Lecointre, B. Viana, Acta Mater. 60 (2012) 6641–6649.

[28] Y.L. Huang, W.X. Zhao, Y.G. Cao, K.W. Jang, H.S. Lee, C. Eunjin, Y. Soung Soo, J. Solid State Chem. 181 (2008) 2161–2164.

[29] Y. Huang, C. Jiang, Y. Cao, L. Shi, H.J. Seo, Mater. Res. Bull. 44 (2009) 793–798.

[30] D.W. Wen, Z.Y. Dong, J.X. Shi, M.L. Gong, M.M. Wu, ECS J. Solid State Sci. Technol. 2 (2013) 178–185.

[31] J.Y. Wang, C. Wang, Y. Feng, H.M. Liu, Ceram. Int. 41 (2015) 11592–11597.

[32] X.Y. Mi, J.C. Sun, P. Zhou, H.Y. Zhou, D. Song, K. Li, M.M. Shang, J. Lin, J. Mater. Chem. C 3 (2015) 4471–4481.

[33] F.Y. Xie, Z.Y. Dong, D.W. Wen, J. Yan, J.X. Shi, J.Y. Shi, M.M. Wu, Ceram. Int. 41 (2015) 9610–9614.

[34] F.Y. Xie, J.H. Li, Z.Y. Dong, D.W. Wen, J.X. Shi, J. Yan, M.M. Wu, RSC Adv. 5 (2015) 59830–59836.

[35] P.W. Zhou, Y.S. Zhu, W. Xu, L. Xu, H.W. Song, Opt. Expr. 21 (2013) 25744–25751.

[36] W.Y. Zhao, S.L. An, B. Fan, S.B. Li, J. Lumin. 143 (2013) 71–74.

[37] P.H. Yang, X. Yu, H.X. Xu, T.M. Jiang, H.L. Yu, D.C. Zhou, Z.W. Yang, Z.G. Song, J. B. Qiu, J. Solid State Chem. 202 (2013) 143–148.

[38] A. Durairajan, D. Balaji, K. Kavi Rasu, S. Moorthy Babu, Y. Hayakawa, M. A. Valente, J. Lumin. 157 (2015) 357–364.

[39] L.L. Han, X.Z. Xie, J.H. Lian, Y.H. Wang, C.W. Wang, J. Lumin. 176 (2016) 71–76.

[40] P.Y. Poma, W.Q. Santos, T.O. Sales, A.S. Gouveia-Neto, C. Jacinto, J. Lumin. 155 (2017) 18–23.

[41] S.W. Long, D.C. Ma, Y.Z. Zhu, M.M. Yang, S.P. Lin, B. Wang, J. Lumin. 192 (2017) 728–733.

[42] M.H. Fan, S. Liu, K. Yang, J. Guo, J.X. Wang, X.H. Wang, Q. Liu, B. Wei, Ceram. Int. 46 (2020) 6926–6933.

[43] D. Wu, Y.G. Xiao, L.L. Zhang, X. Zhang, Z.D. Hao, G.H. Pan, Y.S. Luo, J.H. Zhang, J. Mater. Chem. C 5 (2017) 11910–11919.

[44] M. Zhao, Z.G. Xia, X.X. Huang, L.X. Ning, R. Gautier, M.S. Molokeev, Y.Y. Zhou, Y. C. Chuang, Q.Y. Zhang, Q.L. Liu, K.R. Poeppeimeier, Sci. Adv. 5 (2019) eaav0363.

[45] Y. Sato, H. Kato, M. Kobayashi, T. Masaki, D.H. Yoon, M. Kakihana, Angew. Chem. Int. Ed. 53 (2014) 7756–7759.

[46] C.C. Lin, Y.T. Tsai, H.E. Johnston, M.H. Fang, F.J. Yu, W.Z. Zhou, P. Whitfield, Y. Li, J. Wang, R.S. Liu, J.P. Attfield, J. Am. Chem. Soc. 139 (2017) 11766–11770.

[47] L. Wang, R.J. Xie, Y. Li, X. Wang, C.G. Ma, D. Luo, T. Takeda, Y.T. Tsai, R.S. Liu, N. Hirosaki, Light Sci. Appl. 5 (2016) e16155.

[48] Y.H. Kim, P. Arunkumar, B.Y. Kim, S. Unithrattil, E. Kim, S.H. Moon, J.Y. Hyun, K. H. Kim, D. Lee, J.S. Lee, W.B. Im, Nat. Mater. 16 (2017) 543–550.

[49] Z.B. Guo, B. Milicevic, J.J. Feng, L. Zhou, F. Yao, S.C. Huang, Z.-C. Wu, W.U. Khan, J.X. Shi, M.M. Wu, J. Alloy. Compd. 837 (2020), 155438.

[50] X.F. Wang, X.H. Yan, Y.Y. Bu, J. Zhen, Y. Xuan, Appl. Phys. A 112 (2013) 317–322.

[51] J. Zhou, Z.G. Xia, Opt. Mater. 53 (2016) 116–122.

[52] L. Zhao, D.D. Meng, Y.Y. Li, Y. Zhang, H.Q. Wang, J. Alloy. Compd. 728 (2017) 564–570.

[53] X. Min, M.H. Fang, Z.H. Huang, Y.G. Liu, C. Tang, X.W. Wu, J. Am. Ceram. Soc. 98 (2015) 788–794.

[54] X.J. Zhang, J. Wang, L. Huang, F.J. Pan, Y. Chen, B.F. Lei, M.Y. Peng, M.M. Wu, ACS Appl. Mater. Interfaces 7 (2015) 10044–10054.